CHINESE OPTICS LETTERS

Vol. 21, No. 7 | July 2023

Photonics 60 GBaud PDM-16QAM fiber-wireless 2 × 2 MIMO delivery at THz-band

Weiping Li (李韦萍)[1], Jianjun Yu (余建军)[1,2*], Bowen Zhu (朱博文)[1], Jiao Zhang (张 教)[2], Min Zhu (朱 敏)[2], Chen Wang (王 晨)[1], Wen Zhou (周 雯)[1], Tangyao Xie (谢堂尧)[3], Jianguo Yu (余建国)[3], and Feng Zhao (赵 峰)[4]

[1] Key Laboratory for Information Science of Electromagnetic Waves (MoE), Fudan University, Shanghai 200433, China

[2] Purple Mountain Laboratories, Nanjing 211111, China

[3] Beijing University of Posts and Telecommunications, Beijing 100876, China

[4] Xi'an University of Posts and Telecommunications, Xi'an 710121, China

*Corresponding author: jianjun@fudan.edu.cn

Received February 14, 2023 | Accepted April 18, 2023 | Posted Online July 20, 2023

The terahertz photonics technique has bright application prospects in future sixth-generation (6G) broadband communication. In this study, we have experimentally demonstrated a photonics-assisted record-breaking net bit rate of 417 Gbit/s per wavelength signals delivery in a fiber-wireless converged communication system supported by advanced digital-signal-processing (DSP) algorithms and a polarization multiplexing-based multiple-input multiple-output (MIMO) scheme. In the experiment, up to 60 GBaud (480 Gbit/s) polarization-division-multiplexing 16-ary quadrature-amplitude-modulation (PDM-16QAM) signals are transmitted over 20 km fibers and 3 m wireless 2 × 2 MIMO links at 318 GHz with the bit error rate (BER) under 1.56×10^{-2}. It is the first demonstration to our knowledge of signals delivery exceeding 400 Gbit/s per wavelength in a photonics-assisted fiber-wireless converged 2 × 2 MIMO communication system.

Keywords: terahertz photonics technique; fiber-wireless converged communication; digital signal processing; THz-band; photonics-assisted technique.

DOI: 10.3788/COL202321.073901

1. Introduction

With the development of wireless communication technology, the rapid increase of data traffic and the rapid growth of user services and applications have put forward higher requirements on the speed and bandwidth of wireless communication systems[1–3]. The photonics-assisted fiber-wireless converged system architectures, as an emerging wireless broadband access technology, can provide reliable broadband and multi-gigabit to users to meet the data traffic challenges[2,3]. Moreover, many 100 Gbit/s class data transmissions have been reported at the E-band, the D-band, or the W-band, which are all potential frequency ranges for future broadband backhaul networks[4,5]. Compared with them, the terahertz-band (THz-band, 0.3–10 THz), with abundant bandwidth resources, is able to improve the delivery capability of the communication system[6–11]. Terahertz (THz) photonics is a promising technology for future communication systems due to its unique advantages, which can support high-frequency carrier waves and large adjustable frequency ranges and provide larger bandwidths for data transmission. Also, it can be seamlessly integrated with optical access networks for more efficient and reliable data transmission. However, due to the high atmospheric attenuation of the THz-wave and the susceptibility to interference from the meteorological environment, indoor short-distance transmission is the main application of THz-wave wireless communication[6].

Some high-speed short-range THz-band wireless communication systems have been experimentally demonstrated based on photonics-assisted fiber-wireless converged systems. For example, Wang *et al.* have experimentally demonstrated a 32 Gbit/s signals delivery system over 1.42 m at 450 GHz[9], and Castro *et al.* have demonstrated an over 100 Gbit/s photonic wireless delivery over 0.5 m at the 300 GHz band[10]. In addition, Pang *et al.* have achieved a bit rate of 260 Gbit/s THz-wave delivery system over 0.5 m with multi-channel Nyquist signals[11]. To further improve the bit-rate of the communication system, the combination of wireless multiple-input multiple-output (MIMO) technology and polarization-division-multiplexing (PDM) technology has been proved to exponentially expand delivery capacity[4,11–16].

Table 1 summarizes a series of important achievements that have been successfully achieved regarding the MIMO delivery based on photonics PDM-systems at the THz band[17–24]. For example, Li *et al.* have experimentally demonstrated a

Table 1. Summary of Important MIMO Delivery Achievements Based on Photonics PDM-Systems at the THz-Band.

Ref.	Frequency (GHz)	Net Rate (Gbit/s)	Modulation	Distance (m)
[17]	450	15	PDM-QPSK	1.42
[18]	450	16.8	QPSK	3.8
[19]	370	38.4	DSM-4096QAM	2
[20]	360–430	103.125	PDM-QPSK	1
[21]	375–500	112.15	PDM-QPSK	1.42
[22]	450	106	PDM-PS-64QAM	1.8
[23]	370	103.125	PDM-QPSK	1
[24]	385/435	206.25	PDM-QPSK	3
This work	318	417	PDM-16QAM	3

photonics-assisted fiber-wireless 2 × 2 MIMO delivery system at the THz-band, which can support 15 Gbit/s net bit rate PDM quadrature-phase-shift-keying (PDM-QPSK) signals delivery[17]. By combining multi-carrier frequencies, 6 × 20 Gbit/s PDM-QPSK signals fiber-wireless delivery has also been demonstrated at 375–500 GHz[21]. Recently, Zhang *et al.* have reported a photonics-assisted demonstration of 2 × 103.1 Gbit/s fiber-wireless delivery at 385 GHz and 435 GHz[24]. However, for the systems based on PDM technology described above, on the one hand, PDM-related impairments including polarization crosstalk and polarization-dependent loss significantly degrade the system performance, which requires advanced demultiplexing algorithms for compensation. On the other hand, there are serious nonlinear impairments in photonics-assisted MIMO communication systems. As a result, most of those demonstrations were performed at a bit rate below 300 Gbit/s per wavelength. Also, the wireless distance of delivery is relatively short.

In this Letter, we have successfully achieved a record-breaking net bit rate of 417 Gbit/s per wavelength signals delivery in a fiber-wireless converged communication system with the help of advanced digital-signal-processing (DSP) algorithms and MIMO scheme based on polarization multiplexing. The constant modulus algorithm (CMA) with an MIMO structure is adopted to compensate for the polarization crosstalk and polarization-dependent loss mainly caused by optical fiber delivery. Meanwhile, we also try to discuss the bit error rate (BER) performance with different numbers of CMA taps. In addition, nonlinear equalizers are employed in the receiver offline DSP to compensate for non-linear impairments and further improve the THz-wave system performance. In the experiment, up to 60 GBaud (480 Gbit/s) PDM-16QAM signals are transmitted over 20 km fibers and 3 m wireless 2 × 2 MIMO links at 318 GHz with the BER under 1.56×10^{-2}. To the best of our knowledge, it is the first demonstration of signals delivery exceeding 400 Gbit/s per wavelength in a photonics-assisted fiber-wireless converged 2 × 2 MIMO communication system.

2. Experimental Setup

Figure 1 depicts the experimental setup of a photonics-assisted fiber-wireless converged 2 × 2 MIMO communication system based on polarization multiplexing at the THz band. At the optical transmitter side, two free-running external cavity lasers (ECL1 and ECL2), working at 1549.76 nm and 1552.304 nm respectively, are adapted to emit continuous waves. The frequency stability is typically ±0.3 GHz for 24 hours. The ECL1 emits the 10 dBm continuous waves to drive an I/Q modulator (I/Q MOD) with a 3 dB bandwidth of 40 GHz. The arbitrary waveform generator (AWG, Keysight M8196A) with an 8-bit

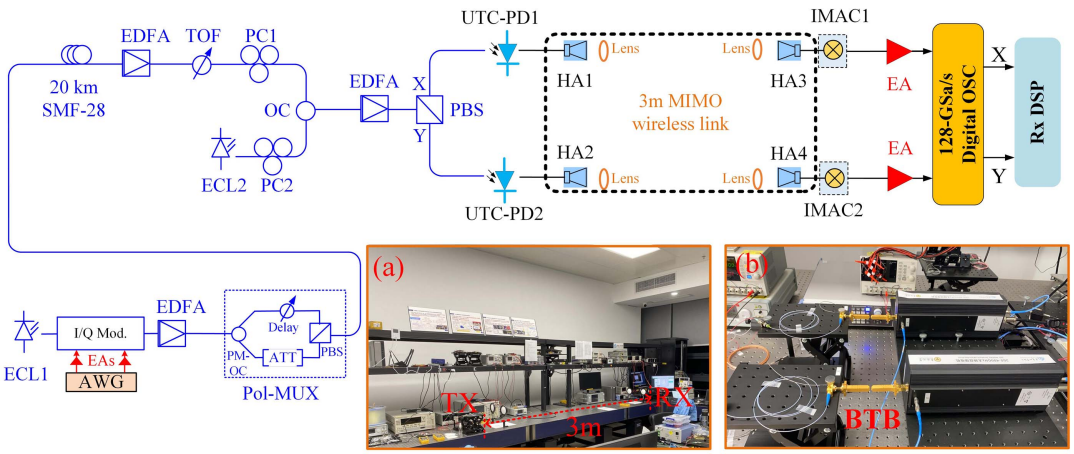

Fig. 1. Experimental setup of the photonics-assisted fiber-wireless converged 2 × 2 MIMO communication system based on polarization multiplexing at the THz band. (a) The scene diagram of the 3-m wireless 2 × 2 MIMO links. (b) The scene diagram of the back-to-back (BTB) wireless link.

vertical resolution and 92 GSa/s sampling rate performs digital-to-analog conversion (DAC) on 60 GBaud 16 QAM signals generated by MATLAB software. The output signals of the AWG are amplified by a pair of electrical amplifiers (EAs) and then delivered into the I/Q MOD to obtain the modulated optical signals. In order to realize polarization multiplexing, the optical signals are transmitted to a polarization multiplexer (Pol-MUX) after being amplified by an erbium-doped fiber amplifier (EDFA). In the Pol-MUX, the optical signals are first divided into two paths by a polarization-maintaining optical coupler (PM-OC). In one path, an optical delay line (DL) of 460-symbol is adopted to remove the correlation of data. In the other path, an attenuator (ATT) is adopted to adjust the power of the optical signals. After that, a polarization beam splitter (PBS) combines the signals transmitted in the two paths to form the PDM signals.

Next, the optical signals are transmitted over a 20 km single-mode fiber (SMF-28). Then, the optical signals pass through an EDFA and a tunable optical filter (TOF) in sequence to compensate for the power loss in the fiber delivery and to suppress the out-of-band amplified spontaneous emission (ASE) noise. Considering that the PBS is sensitive to the polarization state of the signals, a pair of polarization controllers (PC1 and PC2) are adopted to adjust the polarization state of the PDM signals and the local oscillator (LO) signals generated by ECL2. Then, the PDM signals and LO signals are both delivered to an optical coupler (OC) for coupling. In our experiment, we use the method of heterodyne beating to generate THz-wave signals. Figure 2 illustrates the optical spectra of the coupled signals, which have a frequency space of 318 GHz between the LO signals and the PDM signals. For the purpose of controlling the input power into the uni-travelling-carrier photodiode (UTC-PD), an EDFA is used to adjust the power of the coupled signals. Next, we use the PBS to perform polarization diversity on the PDM signals, dividing the coupled PDM signals into *X*-polarized and *Y*-polarized components. Subsequently, the *X*-polarized and *Y*-polarized components are heterodyned in the UTC-PD1 and the UTC-PD2 to generate the THz-wave signals at 318 GHz, which are then transmitted over the wireless 2×2 MIMO links. We use a compact rectangular-waveguide-coupled UTC-PD (280–380 GHz, 100 GHz bandwidth, Model NTT IOD-PMJ-13001) module to achieve the photonic generation of the THz-wave signals[25]. The THz signals converted from the *X*-polarized component are mainly transmitted in channel-1, and the THz signals converted from the *Y*-polarized component are mainly transmitted in channel-2. The structure of channel-1 is the same as that of channel-2, with a couple of horn antennas (HA1–HA4) and a couple of lenses to collimate the THz beam. Figure 1(a) shows the scene diagram of 3 m wireless 2×2 MIMO links.

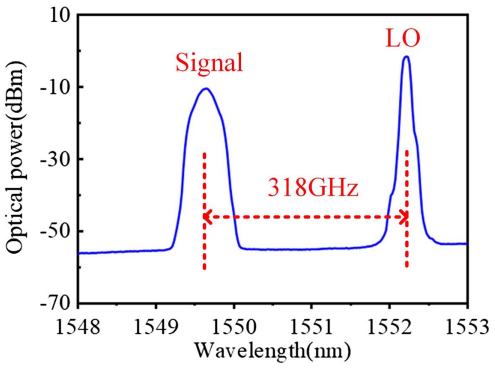

Fig. 2. Measured optical spectra of the 318 GHz optical THz-wave signals.

It is a couple of integrated mixer/amplifier chains (IMAC1 and IMAC2) adopted to down-convert the signals in two channels (channel-1 and channel-2) to the intermediate frequency (IF) signals at about 30 GHz. The IMAC mainly consists of a 14.5 GHz radio frequency (RF) source, a 24× multiplier, amplifiers, and a mixer. After that, the IF signals are amplified by a couple of EAs and later captured by a digital oscilloscope (OSC, 128 GSa/s, Keysight UXR0594A) with a 59 GHz bandwidth and a 10-bit ADC resolution for offline DSP.

3. Digital Signal Processing Routine

Photonics-assisted MIMO communication systems based on polarization multiplexing usually suffer from serious polarization crosstalk, polarization-dependent loss, and nonlinear impairments[26,27]. Considering the polarization rotation generated in the fiber transmission, there is signal crosstalk between the *X*-polarization and *Y*-polarization components after PBS. As a result, each received electrical THz-wave signal contains *X*-polarized and *Y*-polarized signals. Therefore, we adopt the four-butterfly MIMO CMA to eliminate the crosstalk generated in the signal's delivery, including the crosstalk between the *X*-component and *Y*-component after optical fiber delivery. The structure of the four-butterfly MIMO CMA is shown in Fig. 3(a). In addition, the MIMO CMA, as a linear equalization, can realize the dynamic channel equalization and correct the linear damages of the system.

On the other hand, it is also a significant factor for the system performance to be affected by the signal distortion from non-linear disruption. The non-linear distortions are mainly generated from amplifiers, E-O (electrical-to-optical) conversion using an I/Q modulator, O-E (optical-to-electrical) conversion using UTC-PDs based on the technique of photonics-assisted heterodyne beating, and down-conversion after wireless delivery. Non-linear compensation, such as Volterra non-linear equalization (VNLE), is a crucial technology to compensate for non-linear impairments to improve system performance[27,28]. For example, in a coherent optical communication system, Kong *et al.* have successfully applied the VNLE to compensate for the non-linearity in super long-distance optical fiber delivery based on polarization multiplexing and achieved a good improvement in system performance[27]. However, the VNLE has almost never been applied to a photonics-assisted fiber-wireless converged 2×2 MIMO communication system based on polarization multiplexing at the THz band.

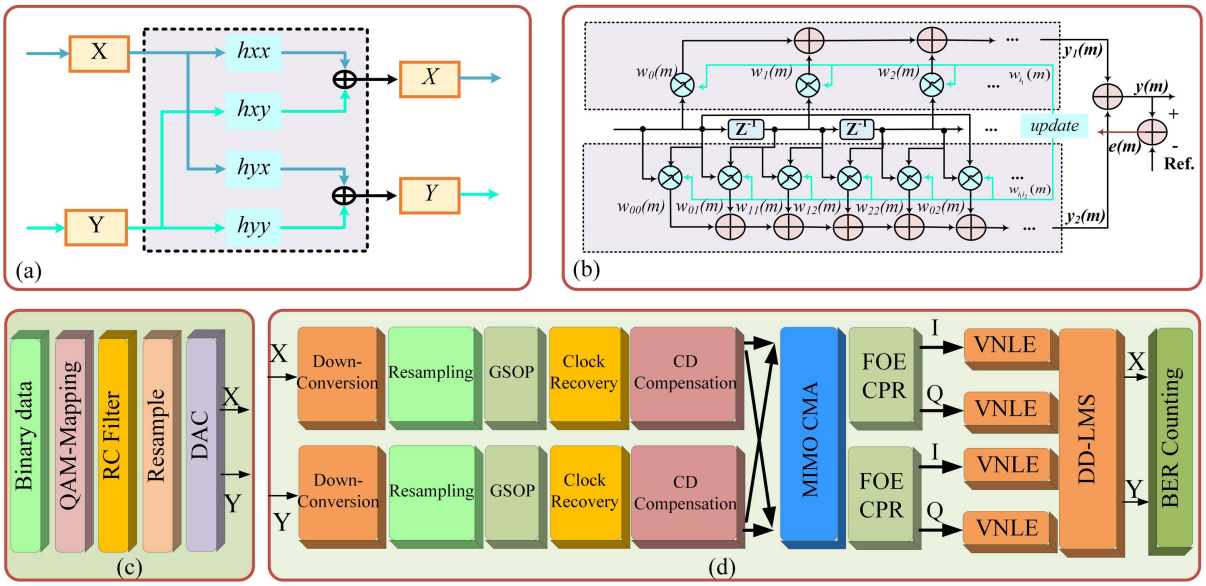

Fig. 3. (a) The structure of the four-butterfly MIMO CMA. (b) The schematic diagram of the non-linear equalizer structure based on the second-order Volterra-series. (c) The DSP routine at the transmitter side. (d) The DSP routine at the receiver side.

In our experiment, the rule of square-law detection is used to realize the photonics-assisted heterodyne beating for THz-wave generation[29]. Therefore, the signal-to-signal beat interference (SSBI) degrades the signal quality. In this case, the high-order (over 2nd-order) non-linear impairment is slight. Moreover, given the complexity of the computation, the second-order Volterra series can be utilized to solve the non-linear problem. Figure 3(b) shows the schematic diagram of the non-linear equalizer structure based on second-order Volterra series we used. Drawing on the method in Ref. [27] to deal with the in-phase/quadrature components of the X/Y-polarized QAM signals while maintaining low computational complexity, we apply four independent VNLEs for four 4-ary pulse amplitude modulation (PAM4) signals included in the 16QAM signals. Thus, it can compensate for the non-linear impairments of each in-phase or quadrature component of the QAM signals.

Figures 3(c) and 3(d) depict the complete DSP routine at the TX-side and RX-side, respectively. In the DSP routine at the TX-side, a string of binary data can be generated by MATLAB/PYTHON software. To offset the bandwidth limitations posed by photoelectric devices, QAM symbols generated after QAM mapping are subjected to raised-cosine (RC) filtering with a roll-off factor of 0.01. This technique can be employed to restrict signal bandwidth within acceptable limits so as to guarantee reliable data transmission. Then, after the QAM symbols are resampled, the DAC is completed in the AWG. The DSP routine at the RX-side mainly includes down-conversion, resampling, the Gram–Schmidt orthogonalization procedure (GSOP), clock recovery, chromatic dispersion (CD) compensation, MIMO CMA equalization, frequency offset estimation (FOE) based on the Viterbi–Viterbi (V–V) algorithm, carrier phase recovery (CPR) based on the blind phase search (BPS) algorithm, the decision-directed least mean square (DD-LMS) algorithm for linear equalization, and BER counting.

Figures 4(a)–4(e), respectively, show the X-polarized signal constellation diagrams after GSOP, after clock recovery, after CMA equalization, after CPR, and after DD-LMS. Figures 4(f)–4(j), respectively, show the corresponding Y-polarized signal constellations. Note that the VNLE is temporarily not used for this process in Fig. 4. Regarding the BER performance improvement of the VNLE, we will show and discuss it in the next section.

4. Experiment Results and Discussion

Figure 5 shows the electrical spectra of the analog-to-digital converted IF signals by using the OSC when the input optical power

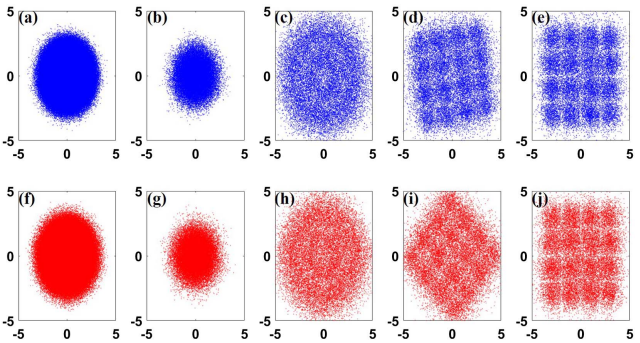

Fig. 4. X-polarized signal constellation diagrams after (a) GSOP, (b) clock recovery, (c) CMA equalization, (d) CPR, and (e) DD-LMS. Y-polarized signal constellation diagrams after (f) GSOP, (g) clock recovery, (h) CMA equalization, (i) CPR, and (j) DD-LMS.

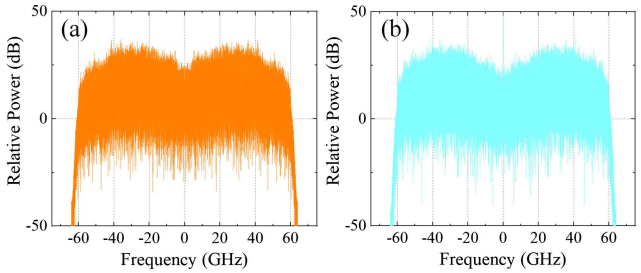

Fig. 5. (a) Electrical spectra of the *X*-polarized signals. (b) Electrical spectra of the *Y*-polarized signals.

of the UTC-PD is 14 dBm. Figures 5(a) and 5(b) correspond to the electrical spectra of the sampled *X*-polarized and *Y*-polarized IF signals after 3 m wireless delivery, respectively.

As shown in Fig. 1(b), the horn antennas are kept very close together, which we call back-to-back (BTB) wireless delivery. In addition, when the OC and the EDFA are connected directly by the optical fiber, we name it BTB optical fiber delivery. For our polarization multiplexed 2×2 MIMO delivery system, we have measured the BER performance of 60 GBaud 16QAM signals in three cases, namely, Case 1 with BTB optical fiber delivery and BTB wireless delivery, Case 2 with BTB optical fiber delivery and 3 m wireless delivery, and Case 3 with 20 km optical fiber delivery and 3 m wireless delivery.

Figures 6(a) and 6(b) illustrate the BERs in different cases for *X*-polarized and *Y*-polarized signals, respectively. For Cases 1–3, increasing the input power into the UTC-PD enhances the BER performance of the signals by improving the signal-to-noise ratio (SNR). Nevertheless, as the input power increases, the radiation power of the UTC-PD is relatively large, and effects such as saturation, noise, and non-linear distortion of the receivers are triggered, resulting in gradual deterioration of the BER performance in Cases 1–3. Therefore, the BER curves depicted in Fig. 6 all show a trend of first falling and then rising. However, due to the power loss incurred during wireless delivery, the required input power in Cases 2 and 3 is much higher than in Case 1 with the same BERs. Furthermore, the BER curves in Case 2 and Case 3 are extremely similar because the EDFA is applied to amplify the optical signals to compensate for the loss of the optical SNR in Case 3. Also, the CD compensation algorithm at the receiver side compensates for the dispersion effect of the 20 km fiber delivery.

Taking the *X*-polarized signal as an example, the BER of the signals reaches a minimum of 1.99×10^{-2} with the 7.2 dBm input power of the UTC-PD in Case 1. Due to the higher requirements of wireless delivery on the radiation power of the UTC-PD, the optimal input power into the UTC-PD in Cases 2 and 3 is 6 dB higher than that in Case 1, and the BERs of the signals reach the minimum values of 1.5×10^{-2} and 1.64×10^{-2} with the 13.2 dBm input power of the UTC-PD in Cases 2 and 3, respectively. In addition, we notice that the minimum BER in Case 1 is slightly higher than that in Cases 2 and 3. The HAs we used in the system have a physical aperture of 3.8 mm × 3.8 mm. This is because high-frequency

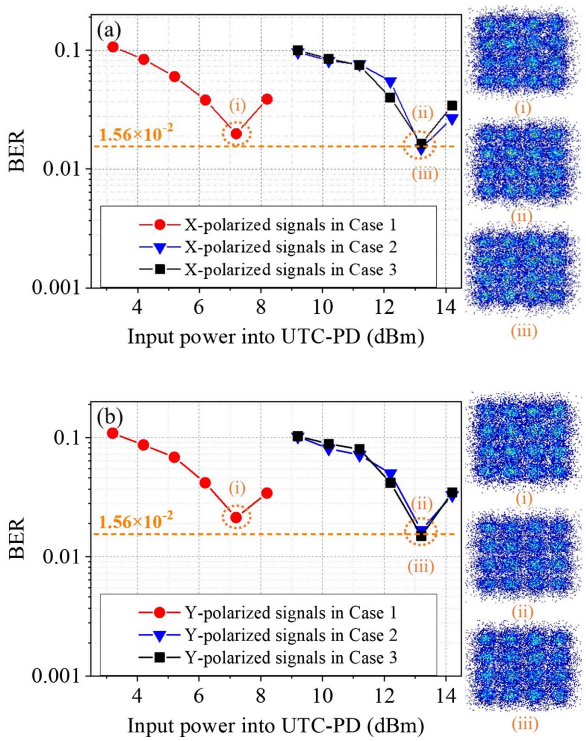

Fig. 6. (a) BER versus the input optical power into the UTC-PD in different cases for the *X*-polarized signals. (b) BER versus the input optical power into the UTC-PD in different cases for the *Y*-polarized signals.

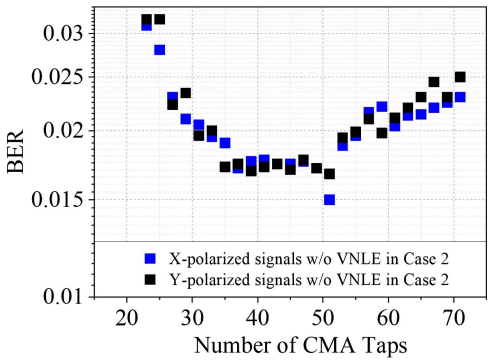

Fig. 7. BER versus the number of CMA taps in Case 2.

THz signals have short wavelengths and strong directionality. When the distance between the transceiver antennas is extremely short, as in Case 1, the system has higher requirements for the alignment of the transceiver antennas. On the other hand, the THz wave may continuously transmit and oscillate between the transmitter and the receiver due to the absence of an isolator, which leads to the BER performance deterioration in Case 1. The constellations after demodulation in different cases for *X*-polarized and *Y*-polarized signals are shown in the insets of Figs. 6(a) and 6(b).

It can be seen from Fig. 7 that the BER performance of the *X*-polarization and the *Y*-polarization components varies with

the number of CMA taps in Case 2. We deploy the CMA taps to eliminate the polarization rotation and distortion generated in fiber transmission. With the increase in the number of CMA taps, the X- and Y-polarization constellations cannot be successfully recovered at first, and it is not until the number of taps reaches 23 that the polarization crosstalk and polarization loss can be accurately estimated, and the X- and Y-polarization constellations can be recovered. When the number of taps continues to increase, the BER characteristics are gradually optimized as the taps length increases. It can be seen that when the number of CMA taps is in the range of 33 to 53, the BER performance is relatively excellent and stable. However, when the number of taps continues to increase, the MIMO CMA tends to converge, which will lead to worse BER performance. This is because the CMA can usually find a more accurate model of the matching channel when using too many taps, which means it captures more transmission channel features. However, using too many taps may capture noise or other irrelevant changes, causing the equalizer's weights to deviate from the optimal solution.

In addition, Figs. 8(a) and 8(b) illustrate the BERs in different cases for X-polarized and Y-polarized signals by utilizing the VNLE in the DSP routine, which is beneficial for further improving the BER performance, since the algorithm can converge on the distribution of constellation points by compensating for the non-linear impairments. Also, the constellations after demodulation in different cases for X-polarized and Y-polarized signals are shown in the insets of Fig. 8. Compared with the BER performance in Fig. 6, we can see that the VNLE can bring a sensitivity gain of ~2.2 dB at the soft-decision forward-error-correction (FEC) threshold of 1.56×10^{-2}. Considering the FEC overhead of 15%[19,22], the net bit rate is $60 \times 4 \times 2/(1 + 15\%) = 417.4$ Gbit/s. In addition, we can notice that BER bounces appear in both Figs. 6 and 8 due to effects such as saturation, noise, and non-linear distortion. Although the VNLE can model and process nonlinearity, it cannot eliminate the root cause of nonlinearity. Therefore, we can notice that BER bounces still appear in Fig. 8, but the magnitude of the bounces is smaller than that in Fig. 6.

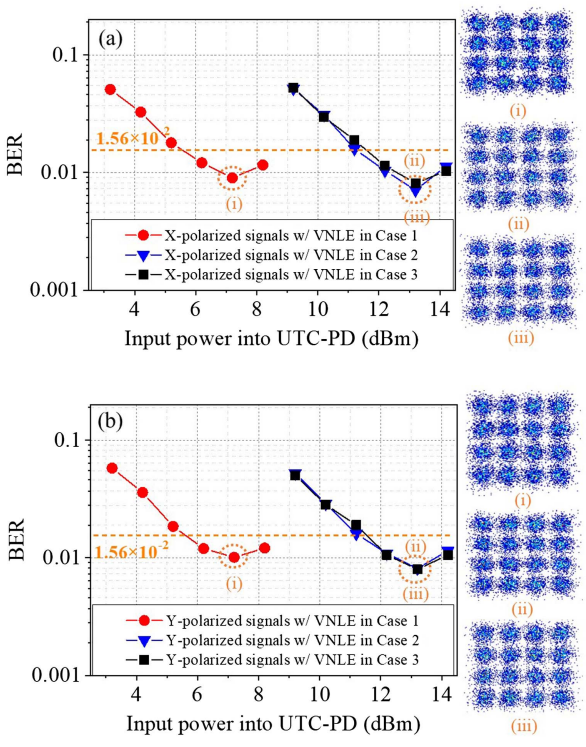

Fig. 8. (a) BER versus the input optical power into the UTC-PD with the VNLE algorithm for X-polarized signals. (b) BER versus the input optical power into the UTC-PD with the VNLE algorithm for Y-polarized signals.

5. Conclusion

We have experimentally demonstrated a photonics-assisted high-capacity fiber-wireless converged 2×2 MIMO communication system at the THz band, in which, for the first time, up to 60 GBaud (480 Gbit/s) PDM-16QAM signals are transmitted over 20 km fibers and 3 m wireless 2×2 MIMO links. With the help of advanced DSP algorithms and MIMO scheme based on polarization multiplexing, a record-breaking net bit rate of 417 Gbit/s signals delivery is experimentally demonstrated after deducting the FEC overhead. To the best of our knowledge, it is the first demonstration of signals delivery exceeding 400 Gbit/s per wavelength in a photonics-assisted fiber-wireless converged 2×2 MIMO communication system. The experiment fully illustrates the bright prospect of photonics-assisted THz band in the aspect of indoor high-capacity fiber-wireless-integrated transmission.

Acknowledgement

This work was partially supported by the National Natural Science Foundation of China (Nos. 61935005, 61835002, and 62127802).

References

1. Z. Ju, J. Liu, and J. Yu, "W-band radio-over-fiber transmission system with delta-sigma modulation and direct detection," Chin. Opt. Lett. **21**, 040602 (2023).
2. W. Li, J. Yu, F. Wang, X. Ji, X. Yang, T. Zheng, Q. Wang, W. Zhou, J. Yu, and F. Zhao, "Photonics millimeter wave bidirectional full-duplex communication based on polarization multiplexing," Opt. Lett. **47**, 6389 (2022).
3. W. Li, J. Yu, Y. Wang, J. Ding, F. Wang, B. Zhu, X. Ji, Y. Tan, T. Zheng, J. Liu, W. Zhou, F. Zhao, and J. Yu, "High spectral efficiency photonics-based polarization multiplexing OFDM signal delivery at W-band," J. Light. Technol. **41**, 4010 (2023).
4. X. Li, J. Yu, J. Zhang, Z. Dong, F. Li, and N. Chi, "A 400G optical wireless integration delivery system," Opt. Express **21**, 18812 (2013).
5. X. Li, J. Yu, and G.-K. Chang, "Photonics-aided millimeter-wave technologies for extreme mobile broadband communications in 5G," J. Light. Technol. **38**, 366 (2020).
6. J. Federici and L. Moeller, "Review of terahertz and subterahertz wireless communications," J. Appl. Phys. **107**, 111101 (2010).
7. H. Zhang, L Zhang, Z Yang, H. Zhang, Z. Lü, X Pan, O. Ozolins, and X. Yu, "Single-lane 200 Gbit/s photonic wireless transmission of multicarrier 64-QAM signals at 300 GHz over 30 m," Chin. Opt. Lett. **21**, 023901 (2023).

8. W. Li, J. Yu, B. Zhu, F. Wang, Y. Tan, Y. Wang, M. Zhu, J. Zhang, W. Zhou, F. Zhao, and J. Yu, "Photonics-aided THz-wireless transmission over 400 m at 335 GHz," Sci. China Technol. Sci. **65**, 3082 (2022).
9. K. Wang, X. Li, M. Kong, P. Gou, W. Zhou, and J. Yu, "Probabilistically shaped 16QAM signal transmission in a photonics-aided wireless terahertz-wave system," in *Optical Fiber Communication Conference* (Optica, 2018), paper M4J.7.
10. C. Castro, S. Nellen, R. Elschner, I. Sackey, R. Emmerich, T. Merkle, B. Globisch, D. Felipe, and C. Schubert, "32 GBd 16QAM wireless transmission in the 300 GHz band using a PIN diode for THz upconversion," in *Optical Fiber Communication Conference* (Optica, 2019), paper M4F.5.
11. X. Pang, S. Jia, O. Ozolins, X. Yu, H. Hu, L. Marcon, P. Guan, F. Da Ros, S. Popov, G. Jacobsen, M. Galili, T. Morioka, D. Zibar, and L. K. Oxenkwe, "260 Gbit/s photonic-wireless link in the THz band," in *IEEE Photonics Conference (IPC)* (IEEE, 2016), p. 1.
12. F. Zhao, J. Yu, and J. Li, "Dual-services generation using an integrated polarization multiplexing modulator," Chin. Opt. Lett. **18**, 110601 (2020).
13. X. Li, Z. Dong, J. Yu, N. Chi, Y. Shao, and G. K. Chang, "Fiber wireless transmission system of 108-Gb/s data over 80-km fiber and 2×2 multiple-input multiple-output wireless links at 100 GHz W-band frequency," Opt. Lett. **37**, 5106 (2012).
14. J. Yu, X. Li, and N. Chi, "Faster than fiber: over 100-Gb/s signal delivery in fiber wireless integration system," Opt. Express **21**, 22885 (2013).
15. X. Li, Y. Xu, and J. Yu, "Over 100-Gb/s V-band single-carrier PDM-64QAM fiber-wireless-integration system," IEEE Photon. J. **8**, 7906907 (2016).
16. Y. Wang, K. Wang, W. Zhou, and J. Yu, "Photonic aided vector millimeter-wave signal generation without digital-to-analog converter," Chin. Opt. Lett. **19**, 011101 (2021).
17. X. Li, J. Yu, K. Wang, W. Zhou, and J. Zhang, "Photonics-aided 2 × 2 MIMO wireless terahertz-wave signal transmission system with optical polarization multiplexing," Opt. Express **25**, 33236 (2017).
18. C. Wang, X. Li, K. Wang, W. Zhou, and J. Yu, "Seamless integration of a fiber-THz wireless-fiber 2×2 MIMO broadband network," in *Asia Communications and Photonics Conference (ACP)* (IEEE, 2018), p. 1.
19. F. Zhao, X. Yang, L. Zhao, Y. Wei, and J. Yu, "Demonstration of 4096QAM THz MIMO wireless delivery employing one-bit delta-sigma modulation," Opt. Lett. **47**, 6361 (2022).
20. J. Zhang, M. Zhu, M. Lei, B. Hua, Y. Cai, Y. Zou, L. Tian, A. Li, Y. Wang, Y. Huang, J. Yu, and X. You, "Real-time demonstration of 103.125-Gbps fiber–THz–fiber 2 × 2 MIMO transparent transmission at 360–430 GHz based on photonics," Opt. Lett. **47**, 1214 (2022).
21. X. Li, J. Yu, K. Wang, M. Kong, W. Zhou, Z. Zhu, C. Wang, M. Zhao, and G. Chang, "120 Gb/s wireless terahertz-wave signal delivery by 375 GHz-500 GHz multi-carrier in a 2 × 2 MIMO system," J. Light. Technol. **37**, 606 (2019).
22. X. Li, J. Yu, L. Zhao, W. Zhou, K. Wang, M. Kong, G. Chang, Y. Zhang, X. Pang, and X. Xin. "132-Gb/s photonics-aided single-carrier wireless terahertz-wave signal transmission at 450 GHz enabled by 64QAM modulation and probabilistic shaping," in *Optical Fiber Communication Conference* (Optica, 2019), paper M4F.4.
23. J. Zhang, M. Zhu, M. Lei, B. Hua, M. Lei, Y. Cai, Y. Zou, W. Tong, J. Ding, L. Tian, L. Ma, J. Xiao, Y. Huang, J. Yu, and X. You, "Real-time demonstration of 100 GbE THz-wireless and fiber seamless integration networks," J. Light. Technol. **41**, 1129 (2022).
24. J. Zhang, M. Zhu, B. Hua, M. Lei, Y. Cai, L. Tian, Y. Zou, L. Ma, Y. Huang, J. Yu, and X. You, "Real-time dual-channel 2 × 2 MIMO fiber-THz-fiber seamless integration system at 385 GHz and 435 GHz," in *European Conference on Optical Communication (ECOC)* (Optica, 2022), paper We2F.4.
25. T. Ishibashi, Y. Muramoto, T. Yoshimatsu, and H. Ito, "Unitraveling-carrier photodiodes for terahertz applications," IEEE J. Sel. Top. Quantum Electron. **20**, 79 (2014).
26. J. Xiao, C. Tang, X. Li, J. Yu, X. Huang, C. Yang, and N. Chi, "Polarization multiplexing QPSK signal transmission in optical wireless-over fiber integration system at W-band," Chin. Opt. Lett. **12**, 050603 (2014).
27. M. Kong, K. Wang, J. Ding, J. Zhang, W. Li, J. Shi, F. Wang, L. Zhao, C. Liu, Y. Wang, W. Zhou, and J. Yu, "640-Gbps/carrier WDM transmission over 6,400 km based on PS-16QAM at 106 Gbaud employing advanced DSP," J. Light. Technol. **39**, 55 (2021).
28. M. Kong, J. Shi, B. Sang, J. Ding, K. Wang, W. Li, F. Wang, C. Liu, Y. Wang, Y. Wei, B. Zhu, L. Zhao, W. Zhou, and J. Yu, "800-Gb/s/carrier WDM coherent transmission over 2000 km based on truncated PS-64QAM utilizing MIMO Volterra equalizer," J. Light. Technol. **40**, 2830 (2022).
29. L. Zhao and J. Yu, "10 Gb/s 16-quadrature amplitude modulation signal delivery over a wireless fiber system by using a directly modulated laser for electrical/optical conversion," Chin. Opt. Lett. **13**, 060601 (2015).